Fluid Dynamics & Materials Processing
DOI:10.32604/fdmp.2020.010150
Article

Analysis of Gas-Solid Flow Characteristics in a Spouted Fluidized Bed Dryer by Means of Computational Particle Fluid Dynamics

Hongming Zhou[1,2], Haozheng Gao[1], Zheng Fang[2], Jiangxin Yang[3] and Mingge Wu[1,2,3,*]

[1]College of Mechanical and Electrical Engineering, Wenzhou University, Wenzhou, 325035, China
[2]Zhejiang Canaan Technology Co., Ltd., Wenzhou, 325000, China
[3]School of Mechanical Engineering, Zhejiang University, Hangzhou, 310027, China
[*]Corresponding Author: Mingge Wu. Email: wmg7810@wzu.edu.cn
Received: 14 February 2020; Accepted: 23 July 2020

Abstract: In order to grasp the particle flow characteristics and energy consumption of industrial fluidized spouted beds, we conduct numerical simulations on the basis of a Computational Particle Fluid Dynamics (CPFD) approach. In particular, the traction model of Wen-Yu-Ergun is used and different inlet conditions are considered. Using a low-speed fluidizing gas, the flow state of the particles is better and the amount of particles accumulated at the bottom of the bed wall becomes smaller. For the same air intake, the energy loss of a circular nozzle is larger than that of a square nozzle.

Keywords: Spouted fluidized bed; CPFD; flow characteristics; numerical simulation

1 Introduction

As a highly efficient reactor, the fluidized bed is widely used in various fields of industry. Pharmaceutical factories use its characteristics of heat and mass transfer to dry particles. At present, the treatment of particles involves gas-solid and liquid-solid flow processes, including physical processes such as transportation, mixing, and drying [1–3]. Therefore, numerical simulation analysis of the structure and process parameters of the fluidized bed is beneficial to optimize the parameters of the fluidized bed and realize industrial scale-up. Scholars have used computational fluid dynamics (CFD) methods and discrete element (DEM) simulations to study the dynamic behavior of flow fields and particles, including the dynamic characteristics of flow fields and particles themselves, and also, the dynamic characteristics of particle interactions. The results are more reliable and authentic. It is difficult to observe the state of the particles. There are complex relationships between particles, such as random movements, collisions and adhesion, which cannot be expressed through quantitative relationships. In the actual operation, it can only be improved through human experience. Numerical simulation can fully show the flow characteristics of particles in the fluidized bed, and provide scientific theoretical guidance for the actual operation parameters and structural improvement.

Spouted bed fluidized bed, as a special form of fluidized bed, has been successfully applied in coal gasification, chemical coating and granulation, and particle drying. There have been many reports on

simulation studies of spouted fluidized beds in the literature. Ding et al. [4] observed the change of density standard of fluidized bed by changing the size of fluidized gas velocity. In the study of the particle mixing characteristics of the spouted bed, Li et al. [5] used the standard deviation of particle characteristic concentration to quantitatively analyze the axial radial mixing quality of the spouted bed. Ren et al. [6] simulated the mixing process of two-component particles with different nozzle velocity and different diameters in a three-dimensional cylindrical cone-shaped spouted bed. Sutkar et al. [7] discussed the influence of nozzle gas velocity and fluidized gas velocity parameters on particle mixing characteristics and pressure drop characteristics using flow pattern diagrams. Li et al. [8] analyzed the influence of different air intake methods on particle mixing characteristics. Zhang et al. [9] used plug-in board technology and CCD for experimental research and introduced the mixing index to study the main mixing mechanism. In the analysis of the influence of the structural factors of the spouted bed on the fluidization, Liu et al. [10] studied the influence of the number of nozzles on the flow pattern. Wu et al. [11] studied the influence of the wind cap distribution on the flow field distribution in the fluidized bed in the air distribution system. Yang et al. [12] studied the influence of the number of cone side sprays and the nozzle diameter on the particle flow in the annulus zone.

CFD has achieved great success in the field of fluids, but there are problems in dealing with a large number of particles in two-phase flow [13,14]. The discrete phase model (DPM) and the discrete element (DEM) discrete element model both have limitations. The DPM ignores particle interactions, while the DEM occupies a lot of computer resources, which makes a limitation on the total amount of particles and cannot reflect the situation in the real fluidized bed.

In this paper, the calculation software Barracuda was used to simulate the fluidization process of fluidized bed particles. The CPFD method based on the MP-PIC (multiphase particle-in-cell) method was used to solve the gas-solid two-phase problem. We analyzed different gas intake methods and different intake shapes to research particle flow characteristics.

2 Numerical Simulation Methods

The characteristic of the MP-PIC method is that it can solve the momentum equation of particles and fluid in three-dimensional space by using the Eulerian method for the fluid phase. The momentum equation is expressed by the Navier-Stokes equation, and the particle phase is processed by the Lagrangian method, in which the position and displacement of particles affect the fluid, and the fluid affects the particles through drag, thereby achieving mutual coupling. The Barracuda software package based on the firm foundation of the MP-PIC description of the particle phase with strong coupling between fluid and particle phases. In the CPFD calculation process, each particle is subjected to a complex external force, and the particles calculated by Barracuda software are not just one particle, but a cluster of particles with similar properties [15]. Particle information is mapped to the Euler system through interpolation operators. The particle stress equation is used to calculate the drag force under the Eulerian system and map it back to the Lagrangian system [16]. The motions of the gas phase and the particle phase are calculated by separate control equations.

2.1 Governing Equations

For the gas phase, the governing equation is:

$$\frac{\partial \theta_f \rho_f}{\partial t} = \nabla\left(\theta_f \rho_f u_f\right) \tag{1}$$

where θ_f is the gas volume fraction, ρ_f is the gas density, t is the time, u_f is the gas flow rate.

Gas-phase momentum equation is:

$$\frac{\partial \theta_f u_f}{\partial \mathrm{t}} + \nabla\left(\theta_f \rho_f u_f\right) = -\frac{1}{\rho_f}\nabla \mathrm{P} - \frac{1}{\rho_f}\mathrm{F} + \theta_f \mathrm{g} + \frac{1}{\rho_f}\nabla\tau \tag{2}$$

where P is the gas pressure, F is the macroscopic stress tensor of the gas, τ is the momentum exchange law of gas and particles in a unit volume.

Particle momentum equation:

$$\frac{du_p}{dt} = D_p(u_f - u_{p)}\frac{1}{\rho_p}\nabla \mathrm{p} + \mathrm{g} - \frac{1}{\theta_p \rho_f}\nabla \tau_p \tag{3}$$

where $\mathrm{u_p}$ is the particle velocity, D_P is the interphase drag coefficient, ρ_P is the particle density, θ_P is the particle volume fraction, τ_p is the particle normal stress.

2.2 Fixed Force Model

Particle normal stress model using particle normal stress is:

$$\tau_p = \frac{10\mathrm{P_s}\theta_\mathrm{p}^{\beta}}{\max\left[\left(\theta_\mathrm{cp} - \theta_\mathrm{p}\right),\ \varepsilon\left(1 - \theta_\mathrm{p}\right)\right]} \tag{4}$$

where $\mathrm{P_s}$ is the material parameter, β is the model-free parameter, from 2 to 5, θ_cp is the volume fractionof densely packed particles, ε is a unique parameter of the order of 10^{-7} magnitude constructed to eliminate singular points in the model.

2.3 Gas-Solid Drag Force Model

Interphase drag function coefficient D_p:

$$D_p = 4.5\frac{\mu_f}{\rho_p r_p^2} f_b \tag{5}$$

where μ_f is the aerodynamic viscosity, r_p is the particle radius, the coefficient f_b is determined by the model. During the gas-solid two-phase flow in a fluidized bed, the gas-solid drag force is the main force.

All drag models calculate a force acting on a particle:

$$\overrightarrow{F_p} = m_p D\left(\overrightarrow{u_g} - \overrightarrow{u_p}\right) \tag{6}$$

where m_p is mass of particle, D is drag function. $\overrightarrow{u_g}$ is gas velocity and $\overrightarrow{u_p}$ is particle velocity.

At present, there are many models for gas-solid two-phase flow. The Gidaspow drag model is a more commonly used model. Considering that the drag coefficients in the rare-phase and dense-phase regions are different, at the particle concentration $\alpha_\mathrm{s} \leq 0.2$ times, for sparse gas-solid two-phase flow, the Wen and Yu equation was used [17]. At the $\alpha_\mathrm{s} > 0.2$ times, it was a dense gas-solid two-phase flow, using the Ergun equation [18,19]. Wen-Yu drag function is written as:

$$D_{WY} = \frac{3}{8}C_d\frac{\rho_g\left|\overrightarrow{u_g} - \overrightarrow{u_p}\right|}{\rho_p r_p} \tag{7}$$

$$C_d = \begin{cases} \dfrac{24}{Re}\theta_g^{-2.65} & Re < 0.5 \\ \dfrac{24}{Re}\theta_g^{-2.65}\left(1 + 0.15Re^{0.687}\right) & 0.5 \le Re \le 1000 \\ 0.44\theta_g^{-2.65} & Re \ge 1000 \end{cases} \tag{8}$$

where D_{WY} is the Wen-Yu drag function and θ_g is gas volume fraction.

Re is calculated as:

$$Re = \frac{2\rho_g r_p \left|\overrightarrow{u_g} - \overrightarrow{u_p}\right|}{\mu_g} \tag{9}$$

where ρ_g is gas density, r_p is the particle radius and μ_g is gas viscosity. ρ_g is the same as ρ_f.

$$D_G = \begin{cases} D_{WY} & \theta_p < 0.75\theta_{cp} \\ \left(D_{Ergun} - D_{WY}\right)\left(\dfrac{\theta_p - 0.75\theta_{cp}}{0.1\theta_{cp}}\right) + D_{WY}0.75 & \theta_{cp} \le \theta_p \le 0.85\theta_{cp} \\ D_{Ergun} & \theta_p \ge 0.85\theta_{cp} \end{cases} \tag{10}$$

$$D_{Ergun} = 0.5\left(\frac{C_1\theta_P}{\theta_g Re} + C_2\right)\frac{\rho_g\left|\overrightarrow{u_g} - \overrightarrow{u_p}\right|}{\rho_p r_p} \tag{11}$$

where D_G is the Gidaspow drag equation. θ_p is solids volume fraction, θ_{cp} is the solidsvolume fraction at close packing, C_1 is a linear coefficient and C_2 is a non-linear coefficient. D_{WY} is the Wen-Yu drag equation. D_{Ergun} is the Ergun drag equation.

3 Model Descriptions

The spouted fluidized bed mainly consists of the bed body and the blower. The main body of the bed is composed of a material warehouse and a diffusion chamber, with an air distribution plate installed at the bottom of the bed. The air distribution plate is provided with air inlets with different apertures. The center of the bottom of the bed has a jet inlet. Fluidized air inlets are evenly distributed around. The fluidized bed is pre-paved with a height of approximately 504 mm.

To reduce the calculation and speed up the calculation, the fluidized bed spouted bed has been simplified, ignoring the possibility of wall tilt in the diffusion chamber. Only the main body of the fluidized bed is retained as the simulation area (as shown in Fig. 1), that is, 800 mm in diameter, the height of 2300 mm, while introducing a section of air inlet with a height of 100 mm and a diameter of 100 mm at the bottom. In CPFD, the division method of the Cartesian grid is used to refine the mesh at the bottom of the bed and the location of the vents.

Four different computational domains of 1000, 10000, 30000 and 80000 were used to analyze the computational accuracy of the mesh under the same operating conditions. Fig. 2 revealed that the pressure decreased across the fluidized bed along the height. The pressure drop of 30000 and 80000 grids exhibited similar trends and were in a good agreement, whereas that of 1000 and 10000 grids were significantly different. Considering the computational cost and accuracy of the simulation, the mesh that consists of 30000 grids was used in this study. The number of meshes after division was 30000, using the non-slip boundary.

According to the other literature [20], the interaction between particles and the wall surface was maintained by normal-to-wall momentum retention 0.3, tangent-to-wall momentum retention 0.99, and

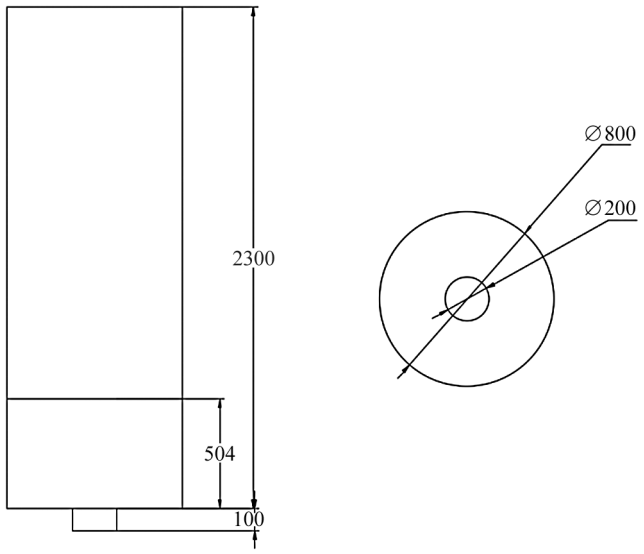

Figure 1: Dimensional drawing of spouted fluidized bed

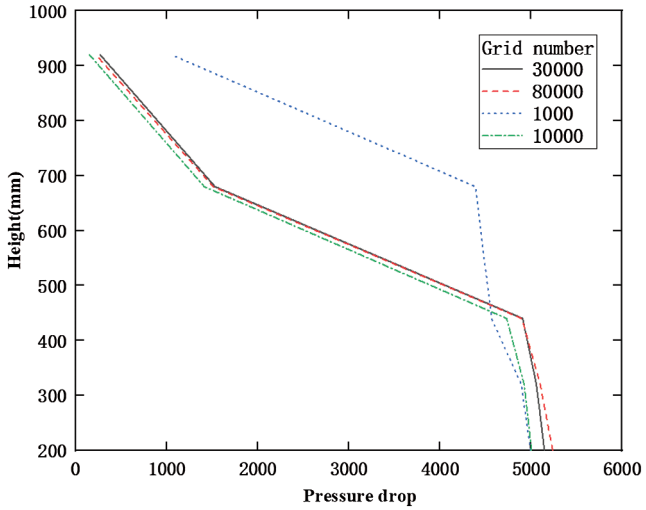

Figure 2: Simulated axial pressure distributions with different grid numbers

Table 1: Parameters of simulated particles

Apparent density	1200 kg/m^3
Particle size	440 μm ∼ 580 μm
Particle size distribution	Evenly distributed
Bulk porosity	0.6

diffuse rebound bounce 0. The particle simulation parameters are shown in Tab. 1, the gas simulation parameters are shown in Tab. 2, and the working condition setting parameters are shown in Tab. 3.

The detailed working condition diagram is shown in the Fig. 3.

Table 2: Parameters of the simulated gas

Density	1.17 kg/m^3
Temperature	300 K
Jet velocity	15 m/s
Fluidization speed	0.25 m/s
Standard atmosphere	101325 *Pa*

Table 3: Parameters of simulation conditions

Working condition 1	Jet velocity 15 m/s Fluidization speed 0 m/ssingle nozzle
Working condition 2	Jet velocity 15 m/s Fluidization speed 0.25 m/sround nozzle + fluidized gas
Working condition 3	Jet velocity 15 m/s Fluidization speed 0.25 m/ssquare nozzle + fluidized gas

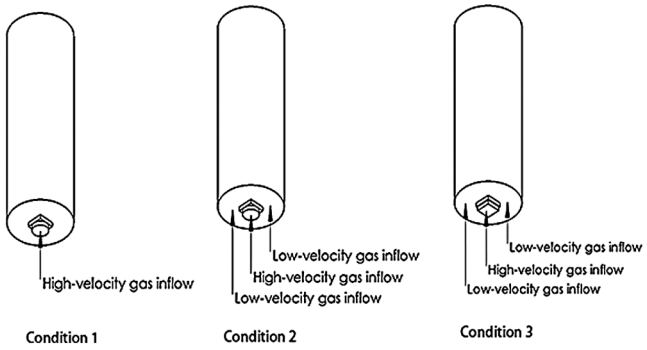

Figure 3: Three different air inlet working conditions

4 Results and Discussions

4.1 Gas-Solid Flow

Under the working condition 1, the model was run for 30 seconds, we select the initial stage as the research stage. Fig. 4 shows the volume particle cloud diagram over time in a fluidized gas-free spouted bed. Visible in the initial 4 s, because the particles at the nozzle did not all reach the minimum fluidization speed, most of the areas are in a static state. A hollow zone was formed at the bottom of the bed. Since the bubbles did not completely penetrate the bed material, the particles upper bed had increased from the initial height, and the volume of the bubbles and the bed material gradually increased. At 6 s, when the air bubbles have reached the upper bed, but did not penetrate the top, the overall height of the bed rise. When the high-speed sprayed gas completely passes through the bed, that is, the center of the nozzle, forming a section of the spring, the blown gas moves to both sides in the axial direction, while the particles are blown to a higher position. The volume fraction on both sides of the bed increases. By 8 s, the overall bubble volume fraction decreases as the bubbles rush out of the bed. When it reached 10 s, a clear spring area, jet area and annulus area were formed. (Note: To represent the mixed characteristics of the particles, Fig. 5 divides the height of the particles into two layers, the upper layer is red and the lower layer is blue).

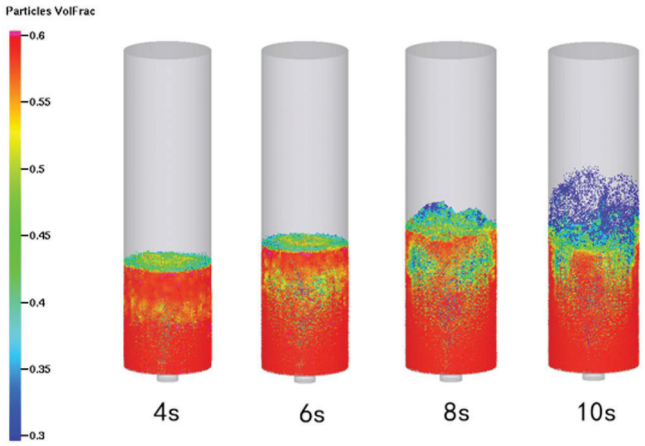

Figure 4: 4–10 s particle volume fraction distribution under working condition 1

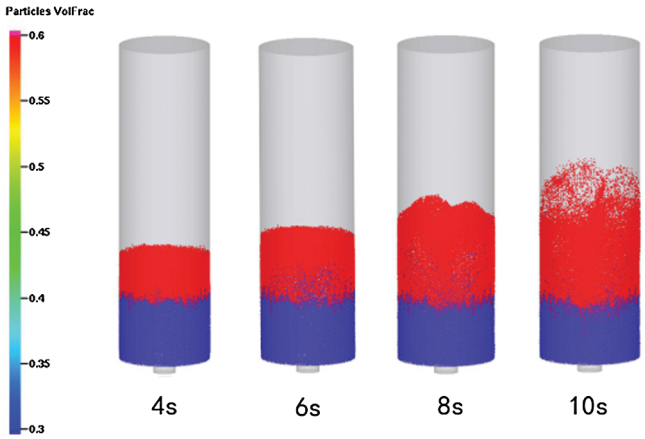

Figure 5: 4–10 s particle composition distribution under working condition 1

Figs. 6 and 7 show the volume fraction and composition cloud diagram over time with the introduction of a fluidized gas spouted bed. The particle volume distribution of the fluidized bed was observed from Fig. 6. Compared with Fig. 4, a low-speed fluidized gas was added around the nozzle at the bottom of the bed. It can be seen from the figure that the distribution of the particles in the vertical direction was more extensive than that in the vertical condition without the fluidizing gas. The area that the particles can reach was higher. Compared with the particle volume distribution chart at 8 s, the case 2 had a larger bubble volume than Case 1. In the vicinity of the height of 600 mm, the particles flow to both sides in the radial direction, and the particle volume fraction of the area is lower. The height of the central fountain increases with the introduction of fluidized gases. It can be explained that low speed fluidized gas is introduced to reduce the flow resistance of the central nozzle. The central spout is strengthened with more force to form a higher fountain. This was consistent with the experimental work of Li et al. [21].

In working condition 2, the fluidizing gas was introduced around, and the circular high-speed gas nozzle was used in the middle. The shape of the nozzle in working condition 2 was improved, that is, a square high-speed gas nozzle with equal area was used for numerical simulation without changing the gas flow rate. Figs. 8 and 9 show the volume particle and composition cloud diagram of the fluidized gas spouted bed with a square nozzle over time.

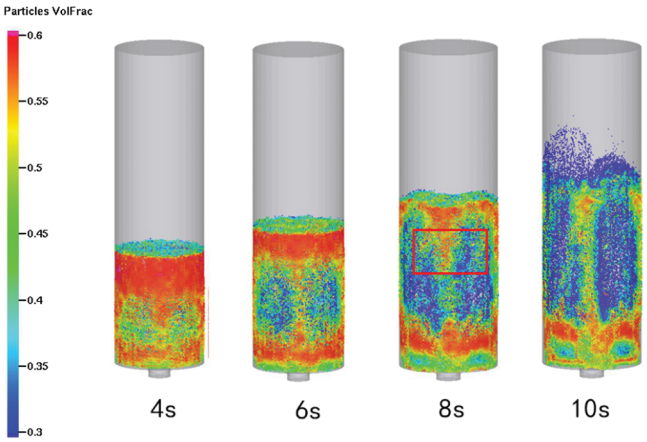

Figure 6: 4–10 s particle volume fraction distribution under working condition 2

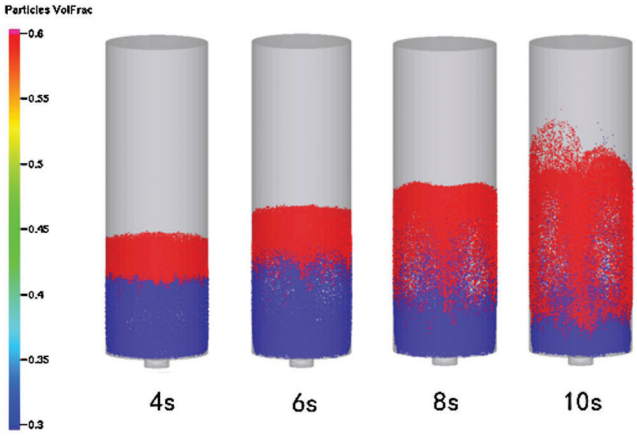

Figure 7: 4–10 s particle composition distribution under working condition 2

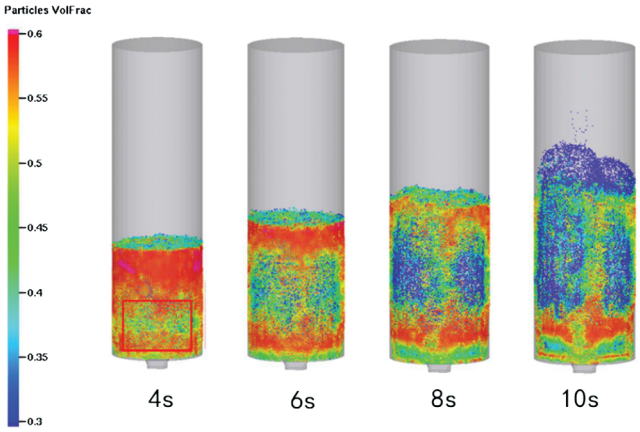

Figure 8: Distribution of particle volume fraction in 4–10 s under working condition 3

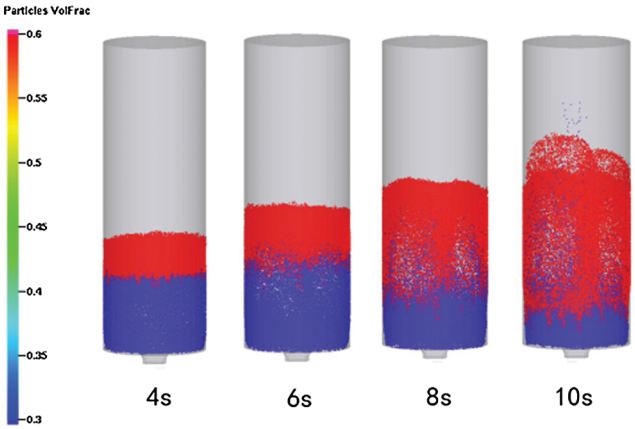

Figure 9: 4–10 s particle composition distribution under working condition 3

Observing the particle volume distribution of the fluidized bed from Fig. 8, and the overall particle flow state was similar to the working condition 2. At 4 s, the particle's volume fraction is lowest near an area with a height of 400 mm. In the area at the bottom of the bed, some particles are suspended. Some of the upper red particles were already inside the blue particles and are already in a mixed state (in Fig. 9).

4.2 Particle Distribution

Fig. 10 shows the distribution of the particle volume along the radial path of the three spouted beds at different bed heights at some point. When the gas passes completely through the material layer of the bed, the material volume of the bed shows a small distribution in the middle and a large distribution on both sides. At the vertical height, the trend of gradual decline is shown, which is manifested in the vertical direction of the nozzle, which is smaller to the sides of the wall, mainly because the bubbles have not yet reached the uppermost bed material, and the volume of the bubbles is getting bigger and bigger. Around the bottom spout, it is a dense area where particles mainly accumulated. Comparing Fig. 10(b) to Fig. 10(a), due to the introduction of fluidized gas around the gas jet, it had a significant effect on the accumulation of particles at the bottom of the bed. Fewer particles are accumulating at the bottom of the bed. From the overall distribution degree, the distribution of the particles in the middle of the bed is more uniform. The

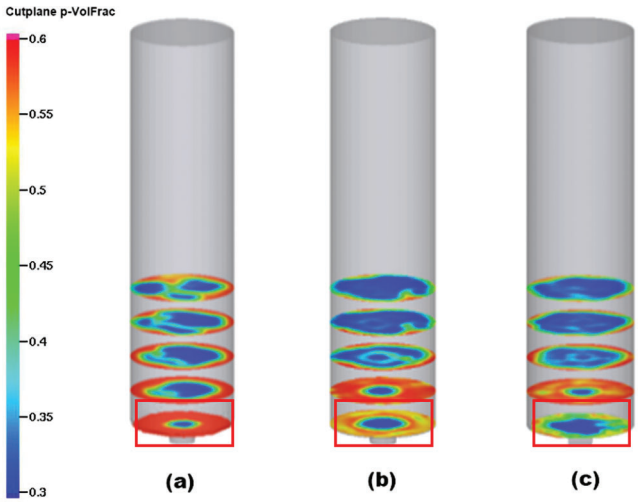

Figure 10: Particle volume fraction distribution

volume fraction of the particles accumulated at the bottom of the bed is smaller. For operating conditions two and three, the overall particle flow condition is not much different. Particles remaining on the walls of the third, fourth, and fifth monitoring surfaces also tend to decrease. At the bottom of the spouted fluidized bed there is a 400 mm dense phase area, similar to the actual spouted fluidized bed. Due to the low-speed fluidized gas, the dead zone of particle accumulation at the bottom cannot be completely destroyed.

Fig. 11 shows the particle flow rate curves flowing through various sections with different air intake methods. After the introduction of fluidizing gas, the average particle flow rate had increased from 540 g/s in working condition 1, to about 660 g/s. The particle flow in the cross-section significantly increased, and the flow of particles at the bottom also increased, conducive to the axial distribution of the particles. Fig. 12 shows the total mass of the axial flow of particle 1. In the second and third working conditions, the lifting amount of particle 1 is greater than the first working condition within the distance near the bottom of the bed (200–800 mm). Fig. 13 is the total mass of the axial flow of particle 2. Before the spouted fluidized bed is not started, particle 2 is distributed on top of particle 1. After the introduction of the fluidizing gas, within 10 s, there is a performance of a large number of particles 2 through the annulus area into the bottom. The degree of inflow of working condition 2 is greater than the other two working conditions, and more conducive to the mixing of particles. It was shown that the introduction of fluidized gas has a positive effect on strengthening the sufficient contact of particles and gas and the uniform distribution of particle groups in the bed (where +, − represents flow direction), which accelerated the mass flow results. The results are similar to the Bayazid's report [22].

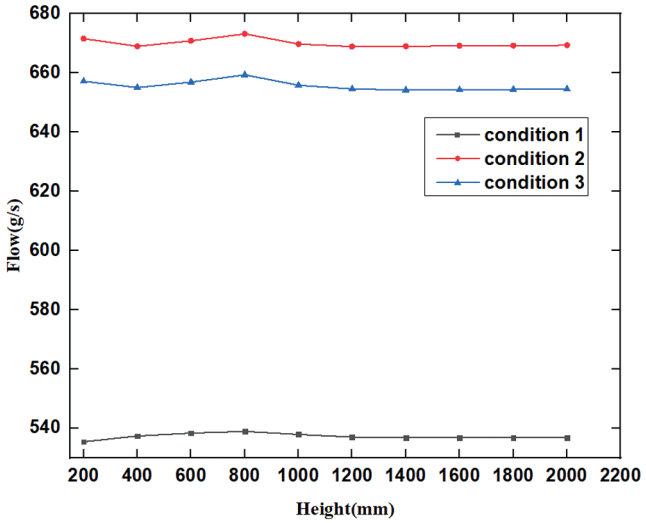

Figure 11: Average axial flow of particles

4.3 Pressure Drop

Five detection points were set at the vertical height at the center of the fluidized bed, and the distance between the detection point and the actual point of the nozzle are 200, 320, 440, 680, 920, 1160 (mm). It can be seen in the change curve of the average pressure drop in Fig. 14 that at the beginning, due to the gravity of the material at the bottom of the bed, the particles need to be fluidized, which required a large amount of energy. Due to the addition of a low-speed fluidizing gas at the bottom, the energy held by the ejection port to support the particles is shared with the fluidizing gas. Near the bottom of the bed, conditions 2 and 3 are greater than condition 1. Due to the two different air intake methods, the degree of gas-solid mixing is enhanced, the energy dissipation is increased, and the total pressure drop of the bed is

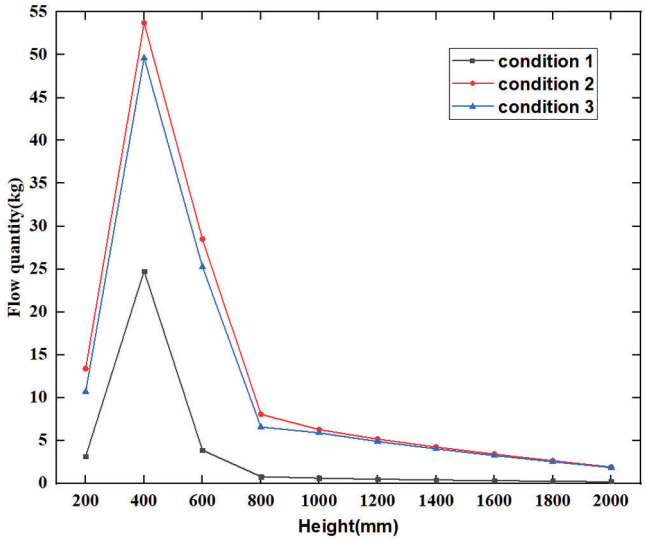

Figure 12: Total mass of axial flow of particle 1

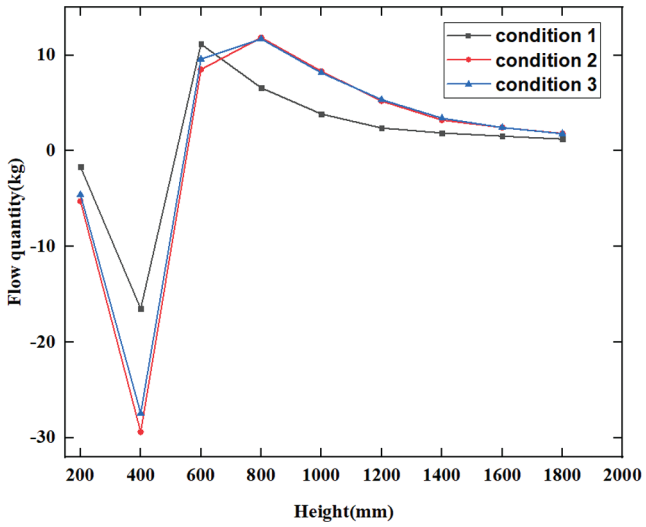

Figure 13: Total mass of axial flow of particle 2

increased, which affects the height of the fountain. This is consistent with Yang's research results [12]. With the same air intake, the pressure drop near the bottom of the bed is manifested in that the circular nozzle has a larger energy loss than the square nozzle. As the height increases, the overall change of the two nozzles is almost the same. From the perspective of the long-term operation of the machine, considering the energy loss of the fluidizing gas, the near-wall area of the bottom surface of the working condition 1 has less volume of gas passing through and less pressure loss. Working conditions 2 and 3 were compared with working condition 1 consumed more energy. Fig. 15 shows the pressure drop loss near the wall. Compared with the central surface pressure drop, the pressure drop loss near the wall surface is slightly smaller. As in the Hosseini's experiment, the pressure loss in the spouting area decreases with height. The pressure drop in the annulus region is obviously lower than that in the spouting region [23].

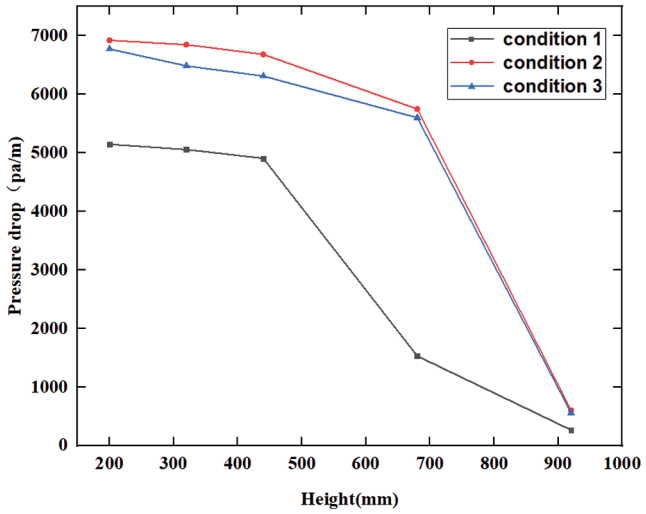

Figure 14: Variation of pressure drop in the center plane

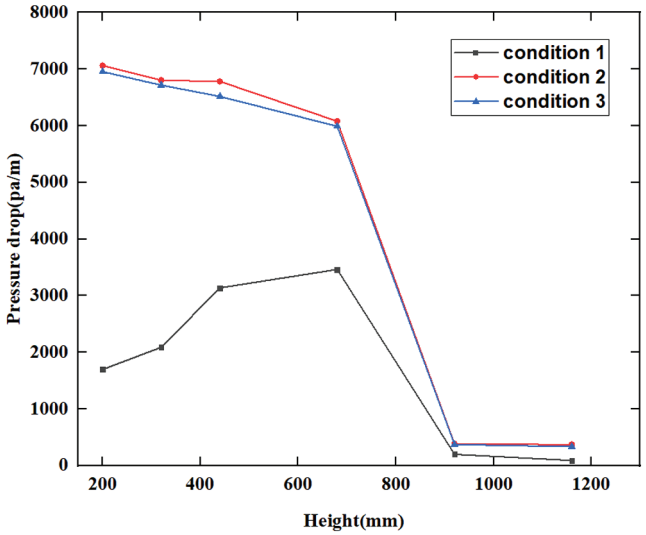

Figure 15: Variation of pressure drop near the wall

5 Conclusion

Based on Barracuda software, the Process of Particles Moving in The Fluidized Bed can be described well by the Wen-Yu/Ergun traction model. Under the same nozzle condition, the appropriate introduction of low-speed fluidized gas can make the dead area at the bottom of the spray fluidized bed significantly improve, so that the number of particles in the air increases, while the number of vertical limit distance stoking the particles be increased, which is of research significance for the drying of particles and the heat transfer at the bottom and top of the fluidized bed.

By introducing the condition of fluidized gas, the radial and axial flow of particles inside the nozzle bed is strengthened, which is conducive to the mixed drying of particles.

Under the condition of introducing fluidized gas, by analyzing the fluidization of the square nozzle and the circular nozzle with the same air intake volume, the overall particle movement process is similar, but the

pressure drop of the circular nozzle near the bottom of the bed is a little larger than square, and the overall flow state of the circular nozzle had a certain advantage over the square nozzle.

Acknowledgement: The authors would like to acknowledge the support provided by the Key Technology Research and Development Program of Zhejiang (2019C01127) and the Natural Science Foundation of Zhejiang Province (LQ20E060012).

Funding Statement: This work was supported by the Key Technology Research and Development Program of Zhejiang (2019C01127) and the Natural Science Foundation of Zhejiang Province (LQ20E060012).

Conflicts of Interest: The authors declare that they have no conflicts of interest to report regarding the present study.

References

1. Aguado, R., Olazar, M., San José, M. J., Gaisán, B., Bilbao, J. (2002). Wax formation in the pyrolysis of polyolefins in a conical spouted bed reactor. *Energy Fuels, 16(6),* 1429–1437. DOI 10.1021/ef020043w.
2. Du, J., Wu, X., Li, R., Cheng, R. (2019). Numerical simulation and optimization of Mid-temperature heat pipe exchanger. *Fluid Dynamics & Materials Processing, 15(1),* 77–87. DOI 10.32604/fdmp.2019.05949.
3. Makibar, J., Fernandez-Akarregi, A. R., Díaz, L., Lopez, G., Olazar, M. (2012). Pilot scale conical spouted bed pyrolysis reactor: draft tube selection and hydrodynamic performance. *Powder Technology, 219,* 49–58. DOI 10.1016/j.powtec.2011.12.008.
4. Ding, S. F., Li, T., Wei, L. B., Li, M. M. (2016). Evaluation of fluidization quality of air heavy fluidized bed. *Journal of Heilongjiang University of Science and Technology, 26(2),* 143–147.
5. Li, B., Song, X. L. (2013). Numerical simulation of particle mixing characteristics in a circulating fluidized bed. *Journal of Power Engineering, 33(10),* 759–764.
6. Ren, B., Zhong, W. Q., Jin, B. S., Yuan, Z. L., Lu, Y. (2012). 3D CFD-DEM numerical simulation of gas-solid flow characteristics in a spouted bed. *Journal of Engineering Thermophysics, 33(8),* 1341–1344.
7. Sutkar, V. S., Deen, N. G., Kuipers, J. A. M. (2017). Spout fluidized beds: recent advances in experimental and numerical studies. *Journal of Power Engineering, 37(2),* 91–97.
8. Li, B., Teng, Z. Y., Zhang, S. B., Wang, Y. T., Ba, X. Y. (2019). Numerical simulation of particle mixing characteristics in a fluidized bed with different inlet methods. *Journal of Power Engineering, 39(2),* 5–91.
9. Zhang, Y., Jin, B. S., Zhong, W. Q. (2008). Experimental study on particle mixing in spouted gas-solid fluidized bed. *Proceedings of the CSEE, 28(20),* 8–14.
10. Liu, R. J., Zhou, Z. Y., Yu, A. B. (2019). CFD-DEM modelling of mixing of granular materials in multiple jets fluidized beds. *Powder Technology, 361,* 312–325.
11. Wu, X., Ma, S. W., Li, K., Zhu, X. F. (2018). Numerical simulation of air distribution system in fluidized bed pyrolysis reactor. *Acta Energic Solaris Sinica, 29(4),* 1038–1044.
12. Yang, C. L., Bai, J. H., Wu, F., Ma, X. X., Yang, J. (2019). Three-dimensional integral spout-fluidized bed structure optimization and flow numerical simulation. *Chemical Journal of Chinese Universities, 33(6),* 1415–1422.
13. Zhang, C., Wu, M. (2019). An analysis of the stretching mechanism of a liquid bridge in typical problems of dip-pen nanolithography by using computational fluid dynamics. *Fluid Dynamics & Materials Processing, 15(4),* 459–469. DOI 10.32604/fdmp.2019.08477.
14. Triveni, M. K., Panua, R. (2018). Numerical study of natural convection in a right triangular enclosure with sinusoidal hot wall and different configurations of cold walls. *Fluid Dynamics & Materials Processing, 14(1),* 21.
15. Zhang, L. D., Wang, Z. J., Li, S. H., Wang, Q., Qin, H. (2018). Computational particle hydrodynamics numerical simulation of the effect of guide tube diameter on spouted bed flow characteristics. *Chemical Engineering & Processing, 37(316),* 21–29.
16. Zhang, R. Q., Yang, H. R., Lv, J. F. (2013). CPFD numerical simulation applied to gas-solid flow and combustion of circulating fluidized bed boiler. *Proceedings of the CSEE, 33(3),* 75–83.

17. Wen, C. Y., Yu, Y. H. (1966). Mechanics of fluidization. *AIChE Journal, 62,* 100–111.
18. Ergun, S. (1953). Fluid flow through packed columns. *Chemical Engineering and Processing, 48,* 89–94.
19. Liu, H. L., Gidaspow, D., Bouillard, J., Liu, W. T. (2003). Hydrodynamic simulation of gas-solid flow in a riser using kinetic theory of granular flow. *Chemical Engineering Journal, 95(1–3),* 1–13. DOI 10.1016/S1385-8947 (03)00062-7.
20. Liang, Y. S., Zhao, X. L., Qin, Q., Guo, Y., Cheng, Y. (2019). CPFD numerical simulation of entrained-flow gasifier. *CIESC Journal, 70(9),* 3291–3299.
21. Li, Y. C., Che, D. F., Liu, Y. H. (2012). CFD simulation of hydrodynamic characteristics in a multiple-spouted bed. *Chemical Engineering Science, 80,* 365–379. DOI 10.1016/j.ces.2012.06.003.
22. Mahmoodi, B., Hosseini, S. H., Olazar, M., Altzibar, H. (2017). CFD-DEM simulation of a conical spouted bed with open-sided draft tube containing fine particles. *Journal of the Taiwan Institute of Chemical Engineers, 81,* 275–287. DOI 10.1016/j.jtice.2017.09.051.
23. Hosseini, S. H., Zivdar, M., Rahimi, R. (2009). CFD simulation of gas-solid flow in a spouted bed with a non-porous draft tube. *Chemical Engineering & Processing, 48(11–12),* 1539–1548. DOI 10.1016/j.cep.2009.09.004.